Science Press

ARTICLE

Electrochemical Properties and Microtopography of 3D Through-Hole Pb-Ca-Sn Anode for Copper Electrowinning

Wang Shuai[1],   Liu Ying[2],   Xu Dong[1],   Zhou Xiangyang[3]

[1] School of Materials Science and Engineering, Hebei University of Engineering, Handan 056000, China; [2] Educational Technology Center, Hebei University of Engineering, Handan 056000, China; [3] School of Metallurgy and Environment, Central South University, Changsha 410083, China

Abstract: 3D through-hole Pb-Ca-Sn anode was prepared which may be a promising anode with excellent performance for copper electrowinning. And the electrochemical properties of 3D through-hole Pb-Ca-Sn anode and Pb-Ca-Sn anode were studied by galvanostatic polarization, electrochemical impedance spectroscopy, anodic polarization and double-Slope Tafel carried out in 160 g/L H_2SO_4 solution at 45 °C. Besides, the micro-morphology, element distribution and phase composition of the oxide layer were investigated. Results show that compared with the traditional Pb-Ca-Sn, 3D through-hole Pb-Ca-Sn anode shows much lower anodic potential, higher exchange current density and better electrocatalytic activity. These characteristics are related to its excellent 3D through-hole structure, which increases the oxygen evolution surface area of the anode. Furthermore, the content of β-PbO_2 and $PbSO_4$ in the oxide layer of 3D through-hole Pb-Ca-Sn is higher and lower than those of Pb-Ca-Sn, respectively.

Key words: 3D through-hole Pb-Ca-Sn anode; anodic potential; oxide layer; copper electrowinning

Copper smelting includes pyrometallurgy and hydrometallurgy, of which hydrometallurgy accounts for about 20%[1]. About 90% of the raw materials for copper smelting comes from sulphide ores, and about 10% comes from oxidized ores and natural copper. The high-grade copper sulfide ore is mainly smelted by pyrometallurgy, while the oxidized copper ore, refractory complex ore and lower grade waste ore are mainly smelted by hydrometallurgy[2]. However, with the rapid development of copper smelting industry and the depletion of high-grade copper concentrate resources, low-grade copper ore, waste ore and refractory composite ore have become the main resources for copper smelting.

Based on the above reasons, the trend of treating copper sulfide ores and copper oxide ores in the hydrometallurgical smelting process with low cost (the cost of hydrometallurgy is about $2000, while $3800 by pyrometallurgy), is increasing with the development of leaching methods and extractants[3]. Moreover, the copper electrowinning is an important step in the whole copper hydrometallurgy process.

At present, the Pb-Ca-Sn alloy has been widely used as insoluble anode for oxygen evolution in copper electrowinning, but it also has some limitations such as high power consumption due to the high oxygen evolution over-potential (OEOP, about 800 mV, accounting for 25%~30% of the total power consumption), unsatisfactory mechanical performance and catalytic activity[4-6].

In order to alleviate those shortcomings, researchers have made a lot of progress in developing new anodes, which can be classified into the following categories. (1) Lead-based alloy plate anode: lead alloy anodes like Pb-Sb, Pb-Cu-Ca-Sn, Pb-Ca-Sn-Al and Pb-Ca-Sn-Co anode[7-9]. (2) Metal coated anodes include Ti matrix, Al matrix and stainless steel matrix anodes like Ti/PbO_2, Ti/RuO_2, Ti/IrO_2-Ta_2O_5, Ti/SnO_2-Sb_2O_3-PbO_2, and Ti/SnO_2-Sb_2O_3-PbO_2-Co_3O_4[10-12], Al/α-PbO_2-β-PbO_2, Al/Pb-Co_3O_4 and Al/Pb-PANI-WC[13-15]; stainless steel/β-PbO_2-TiO_2-Co_3O_4, stainless steel/PbO_2-CeO_2, stainless steel/α-PbO_2-β-PbO_2-CNT and stainless steel/PbO_2-CeO_2[16-18]. (3) 3D structure lead anode such as porous lead anode[19], anti-sandwich structure porous lead anode[20] and 3D Al/Sn rod Pb-Ag anode[21]. (4) Other types of anodes: graphite[22],

polyaniline[23] and porous silicon composite anode[24]. In conclusion, although some progresses have been made in the study of non-lead-based anodes, they are either expensive, complex in preparation, or prone to fall off due to the chemical potential difference between coatings and non-lead substrates. Therefore, lead matrix anode is still widely used in copper electrowinning industry.

According to the Tafel equation, the current density and OEOP will be decreased with increasing the actual surface area of the anode, when the current is constant. Lead foam anode prepared by anti-gravity seepage has good electrochemical performance[25], but its preparation process and mechanical strength need to be improved. Compared with the traditional lead alloy, the anodic potential and OEOP of the porous lead alloy, prepared by our research group with aluminum foam as the pore-making substrate, were greatly reduced, and the electrical conductivity of the anode was greatly improved[26]. However, it is difficult for the anode to completely dissolve aluminum from the precursor, and aluminum will slowly dissolve in the form of ions in the subsequent service process, resulting in electrolyte pollution.

In this study, 3D through-hole Pb-Ca-Sn anode was prepared by infiltration of molten Pb-Ca-Sn alloy into copper foam and the dissolution process of the copper foam from the precursor. After service, the copper foam gradually dissolves into the copper electrolyte. The dissolved copper ions will only slightly increase the concentration of Cu^{2+} in the copper electrolyte, but will not pollute it. Meanwhile, the actual surface area of the anode will be increased and thus the OEOP will be decreased. The electrochemical properties of 3D through-hole Pb-Ca-Sn anode and traditional Pb-Ca-Sn after 72 h galvanostatic electrolysis at the current density of 200 $A \cdot m^{-2}$ were investigated comparatively in 160 $g \cdot L^{-1}$ H_2SO_4 at 45 °C, including anodic polarization, Tafel and electrochemical impedance spectroscopy (EIS). Besides, the phase composition and microscopic morphology of the anode oxide layer were observed by X-ray diffraction (XRD) and scanning electron microscope (SEM), respectively.

1 Experiment

1.1 Preparation of copper foam/Pb-Ca-Sn precursor

The main raw materials were Pb-Ca-Sn alloy (Kunming Hendera Science and Technology Co., Ltd, China) and copper foam (Sichuan Yuantaida Group Co., Ltd., China). The thickness of copper foam was 8 mm and the average pore diameter was about 0.6 mm.

Fig. 1 is a self-made pressurized seepage device, and the entire preparation process consists of the following steps. (1) Turn the left wheel to move the left slider to a specific position and fix it. (2) Rotate the right wheel, and take out the right slider, then the pressurized seepage device was placed vertically, and the copper foam and Pb-Ca-Sn alloy were placed into the seepage chamber. (3) Turn the right wheel so that the right slider just touches the Pb-Ca-Sn alloy, and close the seepage chamber, and then set the heating program to
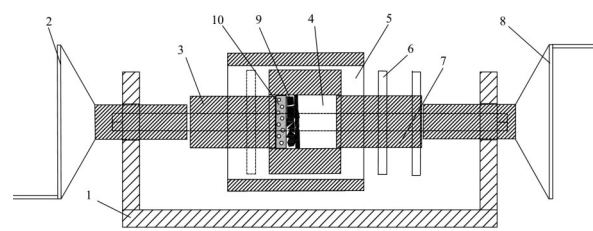

1-pedestal, 2-left wheel, 3-left slider, 4-seepage chamber, 5-heating sleeve, 6-clamping rings, 7-right slider, 8-right wheel, 9-Pb-Ca-Sn alloy, 10-copper foam

Fig.1   Pressurized seepage device of copper foam/Pb-Ca-Sn

make the heating sleeve rise to 450 °C for 15 min. (4) Rotate the right wheel to make the molten Pb-Ca-Sn alloy completely percolate into the copper foam, and hold for 10 min until the copper foam/Pb-Ca-Sn precursor was cooled to room temperature.

1.2 Dissolution of copper foam and preparation of 3D through-hole Pb-Ca-Sn

In the sulfuric acid electrolyte, the copper foam/Pb-Ca-Sn precursor, the stainless steel plate and ammonium sulfate were used as the anode, cathode and complexing agent, respectively. And the change of anode potential with the polarization time was tested. 3D through-hole Pb-Ca-Sn was obtained when the anodic potential was basically stable. The structure of 3D through-hole Pb-Ca-Sn is shown in Fig.2.

The traditional Pb-Ca-Sn and 3D through-hole Pb-Ca-Sn were cut into cubic samples (10 mm×10 mm×8 mm) using a wire-cut machine. Finally, both of them were connected to copper wire and coated by denture base resins with a working area of 10 mm×10 mm. The assembly diagram of experimental sample is shown in Fig.3.

1.3 Measurements

The electrochemical workstation (PARSTAT 4000, Princeton, USA) with three electrode systems was used to measure the electrochemical properties for the anodes in 160 g/L H_2SO_4 solution at 45 °C. The counter electrode was Pt plate (3 cm×3 cm) and the reference electrode was MSE（Hg/ Hg_2SO_4/saturated K_2SO_4）with a potential E_{MSE} = 0.64 V. All potentials in this work are referred to the reference electrode.

Galvanostatic polarization was conducted for 72 h at

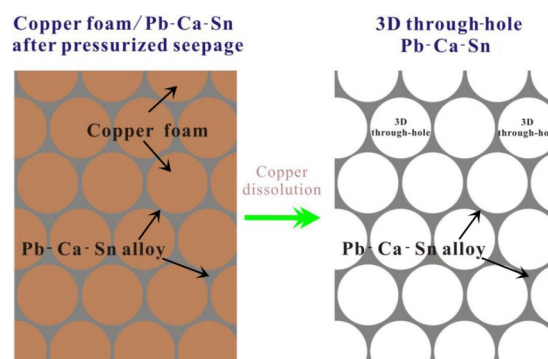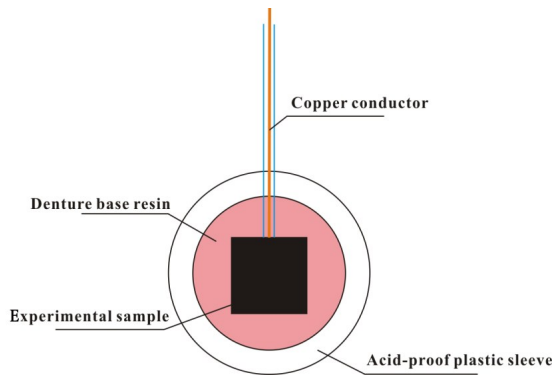Fig.2   Structure diagram of 3D through-hole Pb-Ca-Sn

Fig.3 Assembly diagram of experimental sample

200 A/m^2 in 160 g/L H$_2$SO$_4$ solution. EIS and LSV measurements were conducted immediately after the stable anodic layer was formed by galvanostatic polarization separately. The frequency range of EIS measuring was 0.01~100 kHz and the applied anodic potential for EIS measuring was 1.35 V. The impedance data were fitted to an electrical equivalent circuit (EEC) using the Zview software. The LSV were carried out with the potential ranging from 1.05 V to 1.6 V, and the scanning rate was 5 mV/s.

After galvanostatic polarization, the anodes were taken out, washed with deionized water, and air-dried. Then the morphologies changes and phase transformation of the anodic layers were observed by SEM equipped with energy dispersive X-ray spectroscopy (EDS, Quanta FEG250, American) and XRD (Rigaku-TTRIII, Japan), respectively.

2 Results and Discussion

2.1 Galvanostatic polarization investigations

Galvanostatic polarization test is conducted to confirm the anodic constant potential. Fig. 4 shows the potential-time curves of 3D through-hole Pb-Ca-Sn and Pb-Ca-Sn anodes during the galvanostatic polarization for 72 h.

For Pb-Ca-Sn anodes, the anodic potential in general rapidly decreases, then slightly increases and decreases rapidly until leveling off. At the beginning of the polarization,
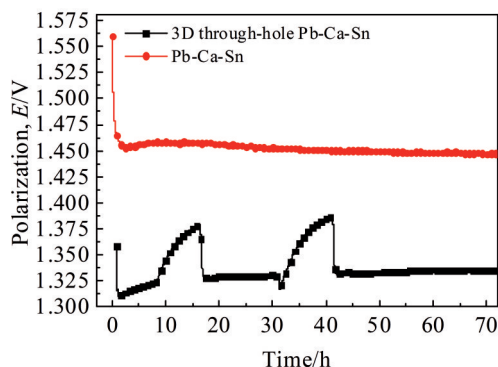

Fig.4 Galvanostatic polarization-time curves of 3D through-hole Pb-Ca-Sn and Pb-Ca-Sn

the anodic potential of Pb-Ca-Sn descends rapidly due to the oxidation reaction of Pb to PbSO$_4$ and following reaction of PbSO$_4$ to the conductive PbO$_2$. With the transformation between Pb, PbSO$_4$ and PbO$_2$, the anodic potential tends to have a slight increase owing to the continuously growing oxide layer. When the generation (Pb/PbSO$_4$ and PbSO$_4$/PbO$_2$) and the decomposition (the corrosion and the oxygen evolution reaction (OER) on the anode surface) of anode layer reach equilibrium, the composition and thickness of oxide layer become stable[27]. Finally, the anodic potential of Pb-Ca-Sn reaches a stable value of 1.45 V.

In general, the galvanostatic polarization curve of 3D through-hole Pb-Ca-Sn is similar to that of Pb-Ca-Sn anode. However, there are two peaks in the galvanostatic polarization curve of 3D through-hole Pb-Ca-Sn at 15 and 40 h. This phenomenon is may be due to the dissolution of residual foamed copper and intense OER, resulting in the growth of fresh oxide layer in 3D through-hole, which can be observed in Fig. 5. In addition, the stable anode potential of the 3D through-hole Pb-Ca-Sn is about 1.333 V, which is 117 mV lower than that of Pb-Ca-Sn at the end of galvanostatic polarization. The different anodic potentials may be explained by the difference in specific surface area of the anodes, directly related to the effective current density in the electrolysis process. Compared with Pb-Ca-Sn, a lower anode potential of 3D through-hole Pb-Ca-Sn is due to its larger specific surface area.

2.2 Microscopic surface morphology and phase composition

In order to study the corrosion morphology and film characteristics of the anodes, the surface micro-topography and element distribution of anodic oxide layer are obtained after 72 h galvanostatic polarization, and the results are shown in Fig. 5. Besides, Fig. 6 depicts the element content of anodic surface corrosion layer.

It can be seen in Fig. 5a and 5c that the anodic layer of 3D through-hole Pb-Ca-Sn consists mainly of tetragonal crystals and orthorhombic crystals with a lot of fine particles and cavities. According to EDS mappings (Fig. 5d~5f), EDS spectrum (Fig. 6) and the following XRD result, the tetragonal crystals are β-PbO$_2$ and the orthorhombic crystals are α-PbO$_2$ phase, probably. This kind of morphology can be attributed to the impact of oxygen evolution and the transformation between PbSO$_4$ and PbO$_2$: (1) the OER occurs not only on the anode surface but also in the 3D through-hole, resulting in a raised number of fine grains and cavities; (2) the conversion of PbSO$_4$ to PbO$_2$ results in a 48% decrease in volume, which is beneficial to the formation of β-PbO$_2$[28]. By comparison, the anodic layer of Pb-Ca-Sn anode shows a irregular crystal structure and possesses some fine grains, as shown in Fig. 5b. Due to the excellent properties of 3D through-hole structure, it is easier for OER to occur.

XRD measurements were used to investigate the composition of anodic oxide layers and the results are shown in Fig. 7. The phase on the oxide layers of the two anodes are
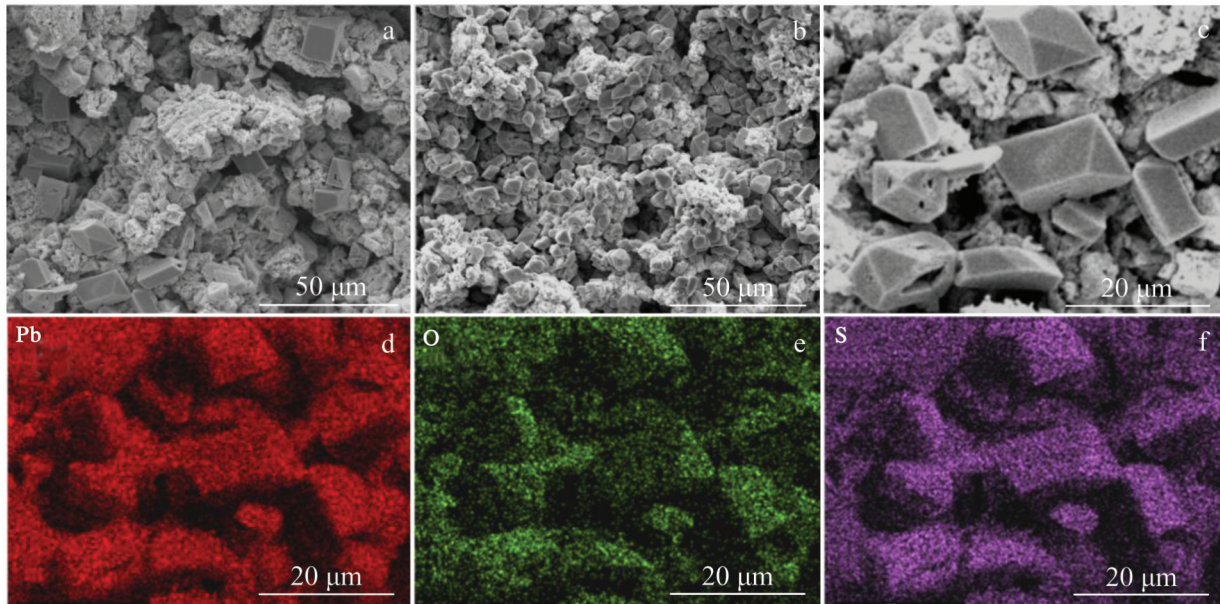
Fig.5   SEM morphologies of 3D through-hole Pb-Ca-Sn (a, c) and Pb-Ca-Sn (b) anodes; corresponding EDS mappings of element Pb (d), O (e), and S (f)
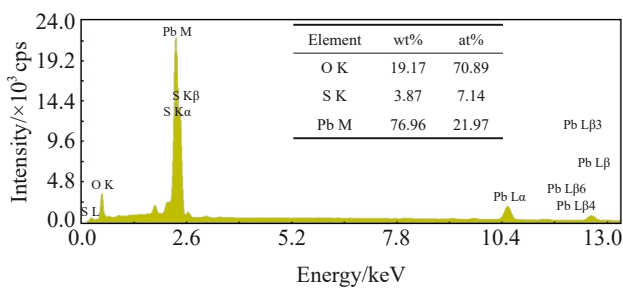

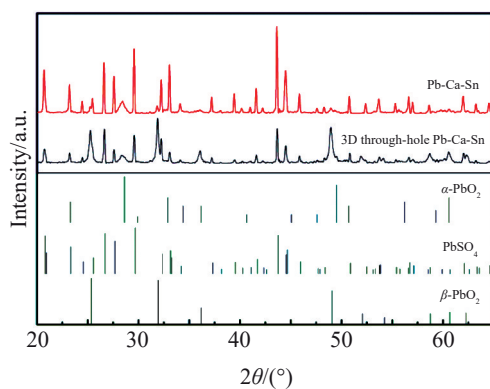Fig.6   EDS results of surface corrosion layer for 3D through-hole Pb-Ca-Sn

Fig.7   XRD patterns of oxide layer of the two anodes after galvanostatic polarization

mainly composed of $PbSO_4$, α-PbO_2 and β-PbO_2. However, the amount of these phases varies between the two anodes.

The major phase of the Pb-Ca-Sn oxide layer is $PbSO_4$ with a small amount of α-PbO_2 and β-PbO_2, while the anodic layer of 3D through-hole Pb-Ca-Sn is determined with β-PbO_2, $PbSO_4$ and a small amount of α-PbO_2, corresponding to the results of the EDS mappings (Fig. 5) and EDS spectrum (Fig. 6). Compared with Pb-Ca-Sn, the diffraction intensity of β-PbO_2 in the oxide layer of 3D through-hole Pb-Ca-Sn is higher while that of $PbSO_4$ is lower, which will result in a lower anode potential[29]. Besides, the 3D through-hole Pb-Ca-Sn oxide layer presents a series of wide and low diffraction peaks, indicating that the grains of anodic oxide layers are amorphous.

2.3 EIS characterizations

Fig. 8 depicts the EIS of the two anodes at 1.35 V. It can be seen that a single capacitance arc can be observed in the whole frequency range, indicating that the electrode reaction mechanism of the two anodes is the same.

The capacitance arc is due to the charge transfer reaction on the surface of electrode. The value of start point and diameter represent electrolyte resistance (R_s) and charge transfer resistance (R_t), respectively. Therefore, a simple R(R-C)
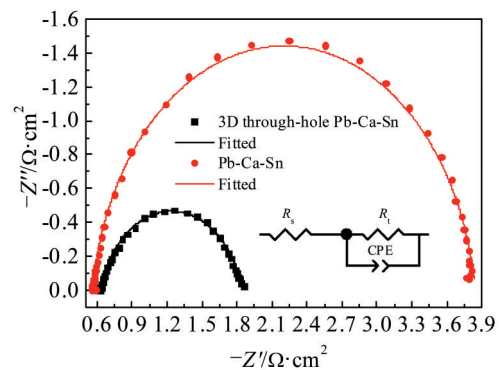

Fig.8   EIS plots and equivalent circuit of the two anodes

circuit can be used as the equivalent circuit to simulate the electrochemical process of the electrode[30,31]. As shown in Fig.8, the experimental (spots) and fitting (lines) data are well-matched, indicating that the equivalent circuit perfectly simulates the electrochemical impedance of the anodes in electrolyte. The parameters are displayed in Table 1.

The double-layer capacitance, C_{dl}, can be calculated from Eq.(1)[32].

$$Q=(C_{dl})^n[(R_s)^{-1}+(R_t)^{-1}]^{(1-n)} \quad (1)$$

Compared with the Pb-Ca-Sn, the R_t of 3D through-hole Pb-Ca-Sn is lower, which may be related to the presence of more β-PbO$_2$ with higher electrocatalytic activity in the anodic surface oxide layer. The C_{dl} of 3D through-hole Pb-Ca-Sn is higher than that of Pb-Ca-Sn, indicating that more oxygen evolution active sites are adsorbed on the surface of the anode. Due to the special structure of 3D through-hole Pb-Ca-Sn, the actual surface area of OER is much larger than that of Pb-Ca-Sn, which is beneficial to the oxygen evolution. In addition, the Q value of 3D through-hole Pb-Ca-Sn is three times larger than that of Pb-Ca-Sn, which means that the electrocatalytic activity of the former is much higher than that of the latter.

2.4 Anodic polarization and kinetic parameters for oxygen evolution

The anodic polarization curves of 3D through-hole Pb-Ca-Sn and Pb-Ca-Sn after 72 h galvanostatic electrolysis are shown in Fig.9. It is very clear that the linear sweep curves of the two anodes present the same basic characteristics. Before the OER, the anode is in passivation state and the current density is low. When the OER begins, the current density increases exponentially with positive potential scanning. The oxygen evolution potentials of 3D through-hole Pb-Ca-Sn and Pb-Ca-Sn are 1.291 and 1.431 V (vs MSE) at a current density of 200 A/m² (0.02 A/cm²), respectively.

In this study, the OEOP (overpotential of oxygen evolution, η) is calculated by Eq.(2)[33]:

$$\eta=E+0.64-1.229-iR_s \quad (2)$$

where E is the anodic potential; 0.64 and 1.229 represent the potential of MSE and OER, respectively; i is the Faradic current; and R_s is the electrolyte resistance, which can be obtained by Table 1. According to Tafel equation ($\eta=a+b\lg i$)[34], a and b can be obtained by linear fitting of the relationship
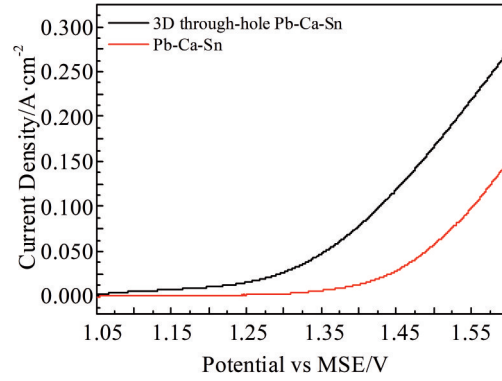

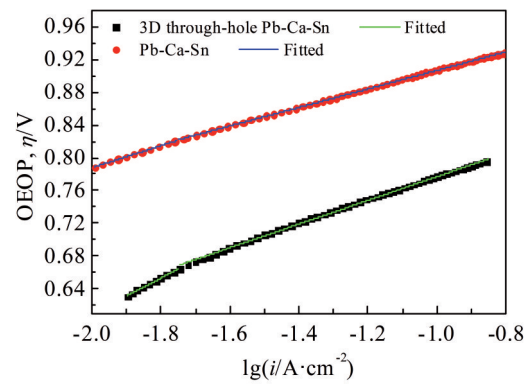Fig.9　Anodic polarization curves of 3D through-hole Pb-Ca-Sn and Pb-Ca-Sn

Fig.10　Tafel lines of the two anodes

curve of η (y-axis) and $\lg i$ (x-axis), and the results are shown in Fig.10. It can be seen in Fig.10 that the Tafel curves of the two anodes are double-slope in the whole potential range. Finally, the exchange current density, i_1 (low potential area) and i_2 (high potential area) can be obtained by Tafel equation when $\eta=0$, and the results are shown in Table 2.

As shown in Table 2, the a values of the two anodes probably depend on the irreversible reactions of PbSO$_4$ to β-PbO$_2$ and α-PbO$_2$ to β-PbO$_2$[35]. The b_1 and b_2 values of 3D through-hole Pb-Ca-Sn are larger than those of Pb-Ca-Sn, which may be because the positive structure of 3D through-hole Pb-Ca-Sn is more conducive to the electrode reaction and OER. The i_1 and i_2 values of 3D through-hole Pb-Ca-Sn are much higher than those of Pb-Ca-Sn, indicating that the former is less susceptible to polarization and the electrode reaction is easier to proceed[36]. As can be clearly observed, the OEOP of 3D through-hole Pb-Ca-Sn is about 0.676 V, which

Table 1　Equivalent circuit parameters of the two anodes

Anode	R_s/ $\Omega \cdot cm^2$	R_t/ $\Omega \cdot cm^2$	Q/ $\times 10^2 \Omega^{-1} \cdot cm^{-2} \cdot s^n$	n	C_{dl}/ $\mu F \cdot cm^{-2}$
3D through-hole Pb-Ca-Sn	0.63	1.214	29.614	0.836	19 615.37
Pb-Ca-Sn	0.563	3.279	8.365	0.922	6 373.77

Table 2　Kinetic parameters of oxygen evolution of the two anodes

Anode	a_1	b_1	a_2	b_2	i_1/A·cm^{-2}	i_2/A·cm^{-2}	η (at 0.02A/cm²)/V η_1	η_2
3D through-hole Pb-Ca-Sn	1.05	0.22	0.92	0.14	1.66×10^{-5}	4.26×10^{-7}	0.675	0.676
Pb-Ca-Sn	1.06	0.13	1.02	0.11	1.37×10^{-8}	9.56×10^{-10}	0.828	0.828

is 152 mV lower than that of Pb-Ca-Sn. This phenomenon may be related to its larger oxygen evolution surface area and higher β-PbO$_2$ content[37].

3 Conclusions

1) Due to the large specific surface area of 3D through-hole Pb-Ca-Sn, its anode potential is about 117 mV lower than that of Pb-Ca-Sn after 72 h galvanostatic polarization. The oxide layer of 3D through-hole Pb-Ca-Sn consists mainly of tetragonal crystals and orthorhombic crystals with a lot of fine particles and cavities. Compared with Pb-Ca-Sn, the diffraction intensity of β-PbO$_2$ in the oxide layer of 3D through-hole Pb-Ca-Sn is higher while that of PbSO$_4$ is lower, which improves the electrocatalytic activity of the anode. The 3D through-hole Pb-Ca-Sn possesses a higher exchange current density, lower charge transfer resistance and oxygen evolution over-potential in comparison with Pb-Ca-Sn. All these characteristics are related to its excellent 3D through-hole structure and high β-PbO$_2$ content.

2) No harmful impurities are introduced and energy saving are realized by the utilization of 3D through-hole Pb-Ca-Sn. Therefore, the developed 3D through-hole Pb-Ca-Sn anode can be used as a high quality material to replace the traditional Pb-Ca-Sn anode.

References

1 H T Yang, Liu H R, Guo Z C *et al*. *Hydrometallurgy*[J], 2013, 140: 144

2 Juan D H, Yuan J G, Jun Y J *et al*. *China Mining Magazine*[J], 2016, 39: 9

3 Zhu Maolan, Tu Tao, Zhu Gensong *et al*. *Rare Metals and Cemented Carbides*[J], 2014, 42: 47

4 Zhang Yongchun, Guo Zhongcheng. *Journal of Alloys and Compounds*[J], 2017, 724: 103

5 Seyedi M, Kosari A, Nakhaie D *et al*. *Journal of Energy Storage*[J], 2018, 17: 442

6 Yuan X T, Lv X D, Hua Z Q *et al*. *Advanced Materials Research*[J], 2011, 402: 351

7 Ivanov I, Stefanov Y, Noncheva Z *et al*. *Hydrometallurgy*[J], 2000, 57: 111

8 Yang B, Cai X, Li E *et al*. *Journal of Solid State Electrochemistry*[J], 2019, 23: 1719

9 Clancy M, Bettles C J, Stuart A *et al*. *Hydrometallurgy*[J], 2013, 131-132: 150

10 Audichon T, Mayousse E, Morisset S *et al*. *International Journal of Hydrogen Energy*[J], 2014, 39(30): 16 785

11 Zhang Cheng, Liu Jianhua, Chen Buming. *Ceramics International*[J], 2018, 44: 19 737

12 Chen S, Chen B, Wang S *et al*. *Journal of Alloys and Compounds*[J], 2019, 815: 152 551

13 Chen Z, Yu Q, Liao D H *et al*. *Transactions of Nonferrous Metals Society of China*[J], 2013, 23: 1385

14 Hu Gang, Xu Ruidong, He Shiwei *et al*. *Journal of Kunming University of Science and Technology (Natural Science Edition)*[J], 2014, 39: 10 (in Chinese)

15 Zhan Peng, Xu Ruidong, Huang Liping *et al*. *Hydrometallurgy*[J], 2012, 125-126: 12

16 Song Y, Wei G, Xiong R. *Electrochimica Acta*[J], 2007, 52: 7024

17 Shi F, Chen B, Guo Z *et al*. *Chinese Journal of Applied Chemistry*[J], 2019, 29: 692

18 Wang X, Xu R, Feng S *et al*. *RSC Advances*[J], 2020, 10: 1355

19 Lai Y, Jiang L, Li J *et al*. *Hydrometallurgy*[J], 2010, 102: 77

20 Jiang L X, Lü X J, Li Y *et al*. *Journal of Central South University (Science and Technology)*[J], 2011, 42: 873 (in Chinese)

21 Chen B, Yan W, He Y *et al*. *Journal of the Electrochemical Society*[J], 2019, 166: 123

22 Panda B, Das S C. *Hydrometallurgy*[J], 2001, 59: 60

23 Hui H, Jiyu Z, Zhihong Y *et al*. *Chemistry*[J], 2010, 3: 277

24 Zhang W, Ghali E, Houlachi G *et al*. *Hydrometallurgy*[J], 2017, 169: 456

25 Lai Y, Jiang L, Li J *et al*. *Hydrometallurgy*[J], 2010, 102: 85

26 Zhou X, Ma C, Yang J *et al*. *Rare Metal Materials and Engineering*[J], 2018, 47: 3009

27 Zhang W, Tu C Q, Chen Y F *et al*. *Journal of Materials Engineering & Performance*[J], 2013, 22: 1677

28 Mohammadi M, Mohammadi F, Alfantazi A *et al*. *Journal of the Electrochemical Society*[J], 2013, 160: 35

29 McGinnity J, Nicol M. *Hydrometallurgy*[J], 2014, 144-145: 135

30 Liu Tingting, Liang Yanhui, Liu Qian *et al*. *Electrochemistry Communications*[J], 2015, 60: 95

31 Zhang Y, Guo Z. *Journal of Alloys and Compounds*[J], 2019, 780: 133

32 Yang H, Guo Z, Chen B *et al*. *Hydrometallurgy*[J], 2014, 147-148: 152

33 Wang Shuai, Zhou Xiangyang, Ma Chiyuan *et al*. *Hydrometallurgy*[J], 2018, 177: 219

34 Lai Y, Li Y, Jiang L *et al*. *Journal of Electroanalytical Chemistry*[J], 2012, 671: 20

35 Hrussanova A, Mirkova L, Dobrev T. *Journal of Applied Electro-chemistry*[J], 2002, 32: 509

36 Zhong X, Yu X, Jiang L *et al*. *JOM*[J], 2015, 67: 2025

37 Dobrev T, Valchanova I, Stefanov Y *et al*. *Transactions of the IMF*[J], 2009, 87: 1

铜电积用 3D-Pb-Ca-Sn 阳极的电化学性能和微观形貌

王　帅[1]，刘　颖[2]，徐　东[1]，周向阳[3]

(1. 河北工程大学 材料科学与工程学院，河北 邯郸 056000)

(2. 河北工程大学 教育技术中心，河北 邯郸 056000)

(3. 中南大学 冶金与环境学院，湖南 长沙 410083)

摘　要： 制备的 3D-Pb-Ca-Sn 阳极有望成为性能优良的铜电积阳极材料。在 160 g/L H_2SO_4 溶液中、45 ℃条件下，采用恒流极化、电化学阻抗谱、阳极极化和双斜率 Tafel 曲线等方法研究了 3D-Pb-Ca-Sn 和传统 Pb-Ca-Sn 阳极的电化学性能。此外，还对 2 种阳极氧化层的微观形貌、元素分布和物相组成进行了研究。结果表明， 3D-Pb-Ca-Sn 阳极具有优良的三维通孔结构，增加了阳极的析氧表面积；因此，与传统的 Pb-Ca-Sn 阳极相比，3D-Pb-Ca-Sn 阳极具有更低的阳极电位、更高的交换电流密度和更好的电催化活性，且其氧化层中 β-PbO_2 含量更高，而 $PbSO_4$ 含量更低。

关键词： 3D-Pb-Ca-Sn 阳极；阳极电位；氧化层；铜电积

作者简介：王　帅，男，1988 年生，博士，副研究员，河北工程大学材料科学与工程学院，河北 邯郸 056000，电话：0310-3967969，E-mail：wangshuai@hebeu.edu.cn